

# General 2.5 power law of metallic glasses

HPSTAR  
270-2016

Qiaoshi Zeng<sup>a,b,c,d,1</sup>, Yu Lin<sup>b</sup>, Yijin Liu<sup>e</sup>, Zhidan Zeng<sup>a,b,d</sup>, Crystal Y. Shi<sup>b</sup>, Bo Zhang<sup>f</sup>, Hongbo Lou<sup>a</sup>, Stanislav V. Sinogeikin<sup>g</sup>, Yoshio Kono<sup>g</sup>, Curtis Kenney-Benson<sup>g</sup>, Changyong Park<sup>g</sup>, Wenge Yang<sup>a,d</sup>, Weihua Wang<sup>h</sup>, Hongwei Sheng<sup>a,i</sup>, Ho-kwang Mao<sup>a,d,g,1</sup>, and Wendy L. Mao<sup>b,c</sup>

<sup>a</sup>Center for High Pressure Science and Technology Advanced Research, Pudong, Shanghai 201203, People's Republic of China; <sup>b</sup>Department of Geological Sciences, Stanford University, Stanford, CA 94305; <sup>c</sup>Stanford Institute for Materials and Energy Sciences, SLAC National Accelerator Laboratory, Menlo Park, CA 94025; <sup>d</sup>High Pressure Synergetic Consortium, Geophysical Laboratory, Carnegie Institution of Washington, Argonne, IL 60439; <sup>e</sup>Stanford Synchrotron Radiation Lightsource, SLAC National Accelerator Laboratory, Menlo Park, CA 94025; <sup>f</sup>School of Materials Science and Engineering & Anhui Provincial Key Lab of Advanced Functional Materials and Devices, Hefei University of Technology, Hefei 230009, China; <sup>g</sup>High Pressure Collaborative Access Team, Geophysical Laboratory, Carnegie Institution of Washington, Argonne, IL 60439; <sup>h</sup>Institute of Physics, Chinese Academy of Sciences, Beijing 100190, China; and <sup>i</sup>Department of Physics and Astronomy, George Mason University, Fairfax, VA 22030

Contributed by Ho-kwang Mao, January 4, 2016 (sent for review December 5, 2015; reviewed by Deok-Soo Kim and Peter K. Liaw)

**Metallic glass (MG) is an important new category of materials, but very few rigorous laws are currently known for defining its “disordered” structure. Recently we found that under compression, the volume ( $V$ ) of an MG changes precisely to the 2.5 power of its principal diffraction peak position ( $1/q_1$ ). In the present study, we find that this 2.5 power law holds even through the first-order polyamorphic transition of a  $\text{Ce}_{68}\text{Al}_{10}\text{Cu}_{20}\text{Co}_2$  MG. This transition is, in effect, the equivalent of a continuous “composition” change of 4f-localized “big Ce” to 4f-itinerant “small Ce,” indicating the 2.5 power law is general for tuning with composition. The exactness and universality imply that the 2.5 power law may be a general rule defining the structure of MGs.**

general structure–property relationship | polyamorphic transition | pressure effect | composition effect | atomic packing

**M**etallic glasses (MGs) possess many unique and superior properties, such as extremely high strength, hardness, and corrosion resistance, etc., making them promising metallic materials with widespread applications (1, 2). Thousands of MGs with a wide range of compositions and properties have been synthesized over the past decades. However, so far the development of MGs is mainly based on tedious composition mapping in multicomponent space to pinpoint the combination of elements with optimized glass-forming ability (GFA). This method for development of MGs is a time- and resource-intensive strategy of trial and error which highlights the need for the guidance of a general theory (2, 3). Intensive research effort has been devoted to finding general rules in various MGs to understand the fundamentals and to guide the development of new MGs (4, 5). Quantitative correlations between their properties have been observed. For instance, compressive yield strength and elastic moduli of MGs are found to be intimately connected with their glass transition temperature  $T_g$  (6–10), and the ductility, fragility (11, 12), and Poisson's ratio of MGs are closely related (13–16). The extensive correlations in properties suggest that the disordered MGs may share general rules in their structure. To clarify this scenario, detailed and accurate structural information spanning short range to long range is required. However, the current experimental probes and theories are limited to local structure in MGs (17). Therefore, understanding how the atoms efficiently fill up the 3D space and how this controls the bulk properties of MGs remains a long-standing theoretical challenge (18–23). To date, few general and exact rules regarding structure–property relationships have been established in MGs (23).

Encouraging progress on understanding structure–property relationships in MGs has recently been made through the discoveries of the noncubic (2.3 or 2.5) power laws that correlate the principal diffraction peak (PDP) position  $q_1$  with the bulk density  $\rho$  or average atomic volume,  $V_a$ , i.e.,  $\rho \propto (q_1)^D$  or  $V_a \propto (1/q_1)^D$ , where  $D$  equals  $\sim 2.3$  with varying the composition of MGs at ambient pressure (19) or  $\sim 2.5$  for tuning the density of MGs with pressure (22, 24). Whereas composition and pressure show similar

exponents in the power laws in MGs, composition and pressure are two independent variables for controlling the density (volume) of materials; they usually have dramatically different effects on MGs. For example, pressure is thought to cause only elastic densification in MGs without obvious structural change because of their already densely packed structure; the structure and properties of MGs are very sensitive to even minor compositional variations (25, 26). In addition, to achieve composition change, different samples usually have to be synthesized. And, many other variables are thought to be inevitably involved, making the compositional change complex (23). Therefore, some basic questions have been perplexing to the glass community: Why do “complex” compositional and “simple” pressure power laws show similar exponents? Is there any connection between them? These questions remain unanswered and have been the major obstacle in understanding the nature of these noncubic power laws.

To address these questions, a systematic study in the 2D pressure–composition space seems to be required. However, the consistency of the data in this kind of study will be questionable. Alternatively, in the present study, we choose the polyamorphous  $\text{Ce}_{68}\text{Al}_{10}\text{Cu}_{20}\text{Co}_2$  MG as a model system. It is well known that Ce-based MG systems show a polyamorphic transition between  $\sim 2$  GPa and  $\sim 5$  GPa caused by the pressure-induced 4f electron localized-to-itinerant transition (27, 28). During this polyamorphic transition, both the atomic size and the electronegativity of Ce are significantly changed (29). Composition tuning in MGs mainly means the variation of atomic size and electronegativity of components, which controls the formation of MGs (30). Therefore, although nothing changes in the nucleus, for MGs this pressure-induced polyamorphic transition is equivalent to a continuous “composition” change with the 4f-localized “big Ce” gradually substituted

## Significance

**This work establishes a general rule correlating the bulk properties [volume ( $V$ )] with atomic structure information (principal diffraction peak position  $q_1$ ) for metallic glasses, i.e.,  $V \propto (1/q_1)^{2.5}$ . It is shown that the 2.5 power law is strictly followed by any metallic glass with its volume tuned by pressure and/or composition. This general 2.5 power law is attributed to the well-constrained structure change/modification that inevitably happens during pressure and/or composition tuning of metallic glasses, which brings insight into the structure of metallic glasses.**

Author contributions: Q.Z., H.-k.M., and W.L.M. designed research; Q.Z., Y. Lin, Y. Liu, Z.Z., C.Y.S., B.Z., H.L., S.V.S., Y.K., C.K.-B., C.P., W.Y., W.W., and H.S. performed research; Q.Z., Z.Z., and H.L. analyzed data; and Q.Z., Z.Z., H.-k.M., and W.L.M. wrote the paper.

Reviewers: D.-S.K., Hanyang University; and P.K.L., University of Tennessee.

The authors declare no conflict of interest.

<sup>1</sup>To whom correspondence may be addressed. Email: qzeng@carnegiescience.edu or hmiao@carnegiescience.edu.

This article contains supporting information online at [www.pnas.org/lookup/suppl/doi:10.1073/pnas.1525390113/-DCSupplemental](http://www.pnas.org/lookup/suppl/doi:10.1073/pnas.1525390113/-DCSupplemental).

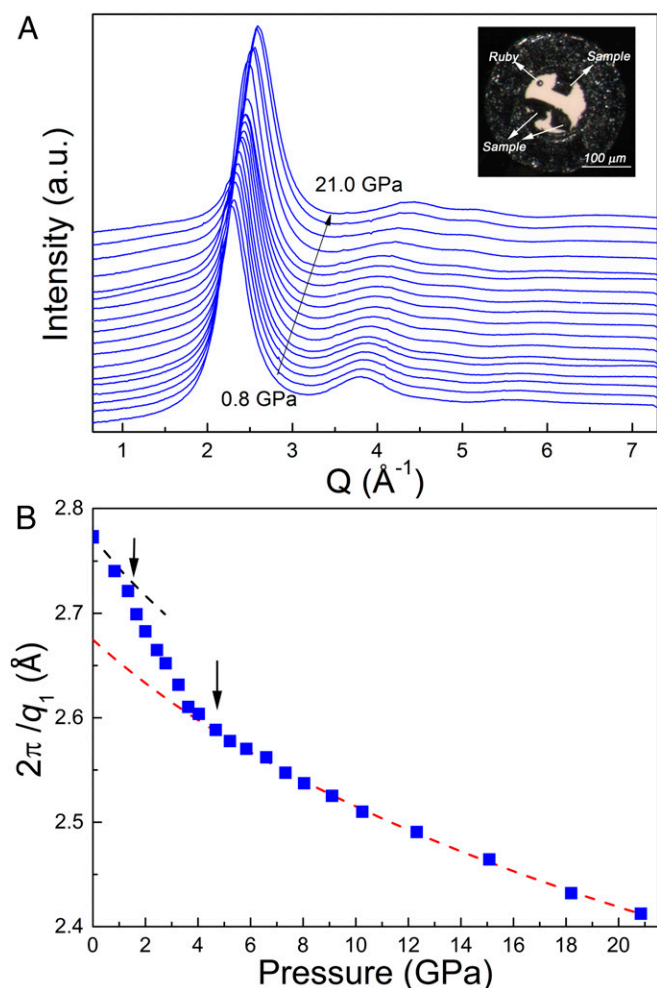


**Fig. 1.** In situ high-pressure XRD measurements of  $\text{Ce}_{68}\text{Al}_{10}\text{Cu}_{20}\text{Co}_2$  MG. (A) XRD patterns from 0.8 to 21.0 GPa. (Inset) Image of samples loaded in a DAC. (B) The  $2\pi/q_1$  versus pressure  $P$  [dashed lines are from the Birch-Murnaghan isothermal equation of state (BM-EOS) fitting in Fig. 3]. Error bars are smaller than the symbol size.

by 4f-itinerant “small Ce.” As a result, we are able to vary both pressure and composition of a MG in a well-controlled way for the first time, to our knowledge.

## Results and Discussion

The  $\text{Ce}_{68}\text{Al}_{10}\text{Cu}_{20}\text{Co}_2$  MG samples were prepared by copper mold casting technique. Using in situ high-pressure X-ray diffraction (XRD) and the recently developed in situ high-pressure full-field nanoscale transmission X-ray microscopy (TXM), the  $q_1$  and volume  $V$  were accurately measured as a function of pressure (see *Materials and Methods* for details). Fig. 1A shows a series of XRD patterns collected in a diamond anvil cell (DAC). Fig. 1B shows the  $2\pi/q_1$  as a function of pressure. The  $2\pi/q_1$  is believed to correlate with the average interatomic spacing in MGs (31–33), which thus could reflect the structural evolution with volume (density) variance under pressure. Two glassy states can be identified in Fig. 1B. They are separated by a transition region between  $\sim 2$  GPa and  $\sim 5$  GPa, indicating a polyamorphic transition in  $\text{Ce}_{68}\text{Al}_{10}\text{Cu}_{20}\text{Co}_2$  MG. This phenomenon is similar to those observed in many other rare-earth-elements-based MGs showing kinks of  $q_1$  under pressure (27, 28, 34, 35).

The sample volume change during compression can be directly measured by TXM, which is proportional to the total number of

voxels within the 3D renderings shown in Fig. 2. The relative volume change  $V/V_0$  as a function of pressure thus can be derived (Fig. 3). A low-density amorphous (LDA) state ( $< \sim 2$  GPa) and a high-density amorphous (HDA) state ( $> \sim 5$  GPa) with a transition region in between can be identified. These results directly confirm the first-order polyamorphic transition from LDA to HDA states with large differences in both the bulk modulus and density (a  $K_0$  increase of 47%, and a density increase of  $\sim 9.6\%$  when extrapolated to 0 GPa) for the first time, to our knowledge. The sample volume changes calculated from diffraction peak positions using the power-law relationship (24)  $V/V_0 \propto (q_1/q_0)^D$  with different exponents ( $D = 3.0$  and  $2.5$ ) are also plotted for comparison. The 2.5 power-law volume data are surprisingly in good agreement with the TXM data (difference is less than 0.4% below 7 GPa) with accuracy comparable to the XRD of crystalline materials, whereas the cubic power law shows increasing deviation with pressure from the TXM volume data (a difference of  $\sim 4\%$  at  $\sim 8$  GPa).

Because both  $q_1$  (Fig. 1) and  $V$  (Fig. 3) are obtained from experiments, with the common variable  $P$ , the relationship between  $q_1$  and  $V$  can be simply established by transfer of variables. Fig. 4A shows the relative volume change ( $V/V_0$ ) as a function of relative  $q_1$  shifting ( $q_1/q_0$ ) in  $\text{Ce}_{68}\text{Al}_{10}\text{Cu}_{20}\text{Co}_2$  MG compared with the data of another three regular MGs from ref. 24. Despite the polyamorphic transition in  $\text{Ce}_{68}\text{Al}_{10}\text{Cu}_{20}\text{Co}_2$  MG, all of the samples including  $\text{Ce}_{68}\text{Al}_{10}\text{Cu}_{20}\text{Co}_2$  MG can be well described by the same 2.5 power law. It thus unambiguously demonstrates that the power-law relationship  $V/V_0 = (q_1/q_0)^{-2.5}$  is strictly and universally followed by any MG with pressure and even compositional change.

The previously reported 2.3 compositional power law is based on the data of different MG samples at ambient pressure (19). To reexamine the compositional power law, we synthesized seven different bulk MGs with large coverage of  $q_1$  from 2.2 to 2.8  $\text{\AA}^{-1}$ . With consistent experimental conditions, the density and XRD of the seven MGs were measured carefully to minimize the experimental uncertainty. The data are listed in Table S1. Fig. 4B shows the comparison of the  $q_1$  versus  $V_a$  obtained in the present work

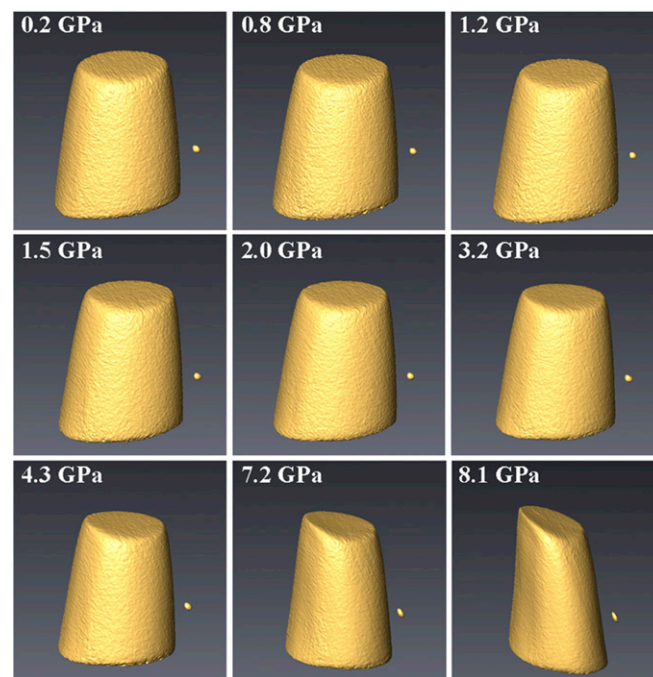


**Fig. 2.** Three-dimensional renderings of reconstructed tomographic data of  $\text{Ce}_{68}\text{Al}_{10}\text{Cu}_{20}\text{Co}_2$  MG at different pressures. A small particle shown beside the sample is the gold fiducial marker.

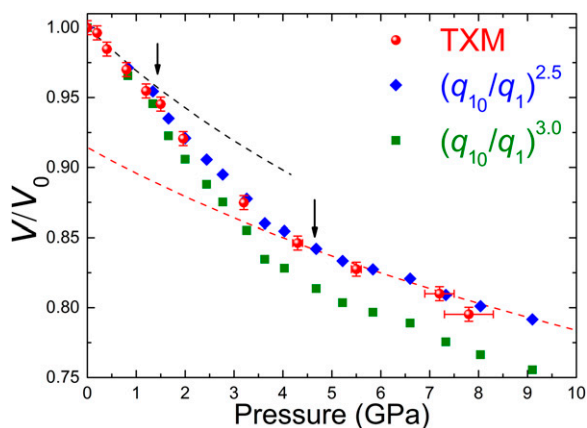


**Fig. 3.** Volume change of  $\text{Ce}_{68}\text{Al}_{10}\text{Cu}_{20}\text{Co}_2$  MG through the polyamorphic transition. Relative volume change ( $V/V_0$ ) obtained by TXM (solid red balls) as a function of pressure compared with the power-law calculations of  $q_1$  (2.5 power law: blue diamonds, 3.0 power law: green squares). The second-order BM-EOS is used to fit the HDA and LDA data, which yields the HDA volume at ambient pressure  $V_{0\text{-HDA}} = (0.912 \pm 0.003) V_{0\text{-LDA}}$  (density  $\rho_{0\text{-LDA}} \sim 6.79 \text{ g/cm}^3$ ), and the HDA isothermal bulk modulus  $K_{0\text{-HDA}} = 48.6 \pm 1.2 \text{ GPa}$  (red dashed line). The black dashed line was simulated by the second-order BM-EOS using experimental value  $K_{0\text{-LDA}} = 33.0 \text{ GPa}$ .

with that from ref. 19. A power-law fitting of the data obtained on the seven MGs yields an exponent of  $2.54 \pm 0.05$ , i.e.,  $V_a = (216.75 \pm 9.64) \cdot (1/q_1)^{2.54 \pm 0.05}$ . This result further confirms that the noncubic 2.5 power law is general for pure composition tuning of MGs. But, it should be noted that in Fig. 4B the data obtained in this work are still embedded in the data set from ref. 19 showing no essential difference between them. Therefore, the refined exponent of 2.5 obtained in our experiments also further confirms the validity of the close noncubic exponent of 2.3 power law obtained based on different data sets in ref. 19.

According to the Debye equation, the XRD static structure factor  $S(q) = (1/N) \sum b_i b_j \sin(qr_{ij})/qr_{ij}$  regardless of the specific atomic structure, where  $N$  is the total number of atoms in the system,  $b_i, b_j$  represent the X-ray scattering length of atom  $i$  and  $j$ , respectively,  $q$  is the scattering vector, and  $r_{ij}$  is the interatomic distance between atoms  $i$  and  $j$ . In an ideal case, if there is only uniform volume scaling down, i.e., all of the interatomic distances  $r_{ij}$  simply shrink by the same rate with the shrunk distance  $r'_{ij} = ar_{ij}$  ( $0 < a < 1$ ), the structure factor will be constant (no phase transition), i.e.,  $S(q') = S(q)$ , then we will have the scattering vector  $q' = q/a$ . This means all of the peak positions in  $S(q)$  will simply shift by the same factor of  $1/a$  in  $q$  space. Thus, the cubic power law  $V_a \propto (r_{ij})^3 \propto a^3 \propto (1/q_1)^3$  will naturally hold if there is no structural transition (e.g., compression of a cubic crystalline phase). This has been the basis of thermal volume expansion measurements in MGs using XRD (33). But, if there is a structural transition (symmetry breaking), the cubic power law will break.

During the polyamorphic transition of the  $\text{Ce}_{68}\text{Al}_{10}\text{Cu}_{20}\text{Co}_2$  MG, pressure and composition are closely associated “equivalent” parameters, which cause the same volume (density) change together. Therefore, the result in this work demonstrates that the 2.5 power law is general for tuning with composition in MGs as well, implying a unified underlying mechanism exists for pressure and/or composition tuning of MGs. Through the polyamorphic transition, there is marked structural change (28). According to the foregoing discussion, this polyamorphic structural change will break down the cubic power law. Hence, obviously the noncubic power law discovered in  $\text{Ce}_{68}\text{Al}_{10}\text{Cu}_{20}\text{Co}_2$  MGs must be intimately associated with the structural change caused by pressure and composition tuning. Moreover, it should be noted that under compression, different element components in a multiple-component MG

system usually have different mechanical responses to pressure; as a result, it will cause structural modifications as well (36). Meanwhile most compositional variation in MGs involves considerable structural change (37). Structure change is a common variable inevitably involved in the composition or pressure tuning of MGs.

Therefore, it is reasonable that the cubic power law breaks down during the pressure and/or composition tuning of MGs, but the exactness and universality of the alternative noncubic (2.5) power law are surprising. It implies that the structural change in MGs is not random, but follows a general, strict rule, which defines the 2.5 power law. Next, why is the structure change of MGs strictly constrained rather than random? In contrast to the open network structure of conventional glasses constrained by charge neutrality and directional covalent bonding, MGs have more degrees of freedom with nondirectional metallic bonding. The structure of MGs is packing-dominated; efficient, dense packing of various atoms/clusters is one basic structural feature [e.g., the density difference between the glass and its crystalline counterpart is often less than 0.5% in MGs (38), whereas it can be up to  $\sim 20\%$  in  $\text{SiO}_2$  network glass (39)]. To achieve the densest possible packing of

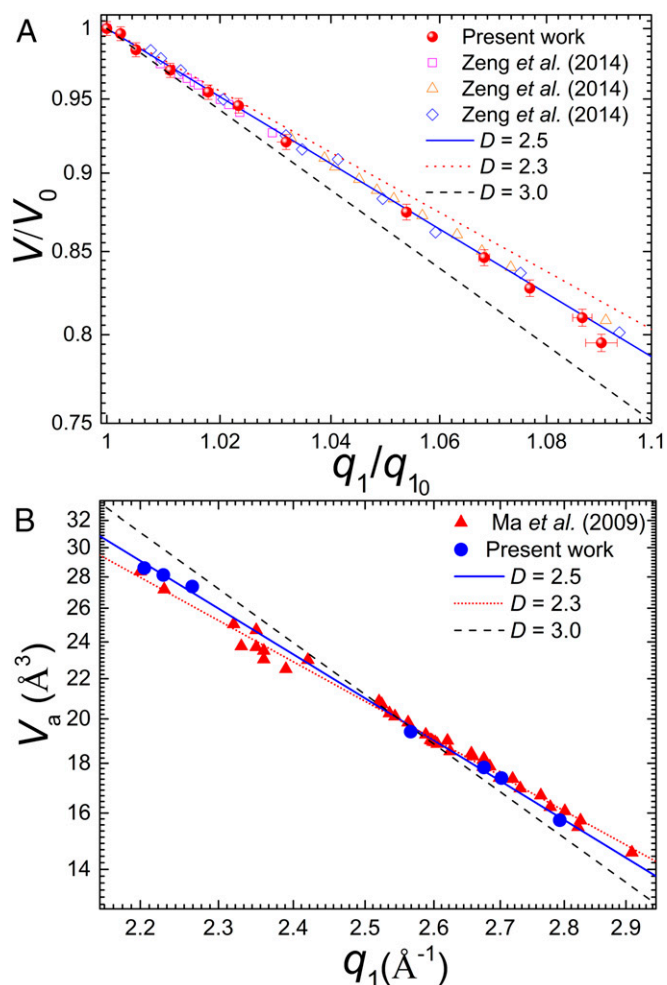


**Fig. 4.** General 2.5 power law for  $V$ - $q_1$  in MGs. (A) Relative volume change ( $V/V_0$ ) as a function of relative  $q_1$  shifting ( $q_1/q_{10}$ ) in  $\text{Ce}_{68}\text{Al}_{10}\text{Cu}_{20}\text{Co}_2$  MG through its polyamorphic transition. Data of other regular MGs from ref. 24 are plotted for comparison. (B) Average atomic volume  $V_a$  versus  $q_1$  tuned by composition. The data obtained in the present work (blue circles) are compared with the data from ref. 19 (red triangles). The 2.3 power law and cubic power law are shown in dotted line and dashed line, respectively, for comparison. Axes in A and B are all shown in a logarithmic scale.

atoms of different sizes, it has been recognized that well-developed local order (e.g., short-range order and medium-range order) are required, which thus rules out the possibility of totally random packing (40). From the chemistry perspective, optimizing the combination of atoms with different sizes and concentrations is the major strategy to improve GFA via achieving efficient packing (3, 41). It means that the composition change/selection of MGs should also follow a certain rule rather than a random combination. Under pressure, the atomic size of each component usually will be changed, especially the size ratio between each component, which is similar to the compositional change and should be constrained as well. Therefore, randomness does not really facilitate the formation of MGs; a hidden general rule may intrinsically exist and play an important role to constrain the structure change of MGs regardless of the origins of the change, e.g., caused by composition and/or pressure. And, this constraint relating the GFA with structure may be manifested as the general and strict 2.5 power law as we observed in experiments. In other words, the 2.5 power law may be the general rule defining the intrinsic feature of MGs.

What kind of specific intrinsic feature might it be? Because the exponent of  $\sim 2.5$  in a power-law relationship characterizes many naturally occurring random fractal systems, such as the diffusion-limited aggregation (42), percolation clusters (43), etc., the general 2.5 power law revealed in MGs may imply an intrinsic fractal packing hidden in their “disordered” structure, and the fractal nature (the particular dimensionality of 2.5) could be intact during composition and/or pressure tuning as long as the samples are still in glassy states. (19). Based on molecular dynamics simulations, this specific fractal structure with dimensionality of  $\sim 2.5$  in MGs has been suggested to be the percolation clusters (22). However, we note that the work in ref. 22 only considered compressional behavior. No connection between pressure and composition tuning of MGs, the focus of the present work, was made.

## Conclusions

In this work, we directly measured the volume  $V$  and diffraction peak position  $q_1$  of the  $\text{Ce}_{68}\text{Al}_{10}\text{Cu}_{20}\text{Co}_2$  MG through its first-order polymorphic transition, and of seven MGs with different compositions at ambient pressure. The pressure and/or composition tuning of MGs all strictly obey the same 2.5 power law, revealing a similar nature. Therefore, a general rule (the 2.5 power law) correlating the structure with properties of MGs is established. The well-constrained structure change during pressure and/or composition tuning is suggested to be the mechanism of this general rule. The dimensionality of 2.5 implies the fractal nature of MG structure. The 2.5 power law may be a necessary and sufficient condition for defining an MG system from the structural perspective which sets them apart from other totally disordered or highly ordered systems. The results in this work may have important implications for understanding the structure of MGs, and even the disorder packing problems in general.

## Materials and Methods

MG rods with a diameter of 1–2 mm were prepared by copper mold casting. The glass nature of prepared rods was examined by XRD and differential scanning calorimetry. Sample densities at ambient conditions were measured

using the Archimedes principle on an analytical balance (Mettler Toledo-XS205DU) with accuracy of 0.01 mg.

In situ high-pressure angle-dispersive XRD experiments with a wavelength of 0.3738 Å and a focused beam size of approximately  $6 \times 7 \mu\text{m}^2$  were performed at beamline 16-ID-B of the High Pressure Collaborative Access Team (HPCAT), Advanced Photon Source (APS), Argonne National Laboratory (ANL). The samples were all cut into approximate  $50 \times 50 \times 20\text{-}\mu\text{m}^3$  chips, and then were loaded into a symmetrical DAC along with a tiny ruby ball beside the sample as a pressure calibrant (44). The gasket was T301 stainless steel. Helium was loaded in a DAC at sector 13, APS, ANL as the pressure-transmitting medium. The pressure fluctuation estimated from the pressures measured before and after each exposure was found to be less than 0.2 GPa. The background scattering was collected at each pressure by shining the X-ray beam on the empty area inside the sample chamber, which only went through helium and two diamond anvils. The XRD measurements of the seven ambient MG samples were performed without DAC but using the same experiment setup with in situ high-pressure XRD experiments.

The TXM experiments were performed at beamline 6-2 of the Stanford Synchrotron Radiation Lightsources (SSRL), SLAC National Accelerator Laboratory. To simplify the experiment and the reconstruction, the  $\text{Ce}_{68}\text{Al}_{10}\text{Cu}_{20}\text{Co}_2$  BMG sample was cut into a nearly cylindrical shape ( $\sim 15 \mu\text{m}$  in height and  $\sim 10 \mu\text{m}$  in diameter) with high-quality surface using focused ion beam (FIB) in the Stanford Nanocharacterization Laboratory (FEI Strata 235 Dual-Beam FIB/SEM). A beryllium (Be) gasket with cubic BN/epoxy insert was prepared, which can reliably maintain the thickness of the sample chamber above  $30 \mu\text{m}$  up to 20 GPa (24). Silicone oil was loaded into a cross-DAC as the pressure-transmitting medium with two tiny ruby balls close to the sample as the pressure calibrant. Some gold fiducial markers were loaded as well beside the sample for accurate alignment in the tomographic reconstruction. The full-field TXM was used for tomography data (2D projection images) acquisition. The field of view was  $\sim 40 \mu\text{m}$  while the 2D spatial resolving power of the microscope is better than 40 nm. The sample was illuminated by a 9.4 keV conical X-ray beam created by a capillary condenser. The raw 2D projection images of  $2,048 \times 2,048$  pixels were collected every degree with the exposure time of 10 s during sample rotation from  $-90^\circ$  to  $90^\circ$  (examples are shown in Fig. S1). Then the raw 2D images were processed using TXM-Wizard software (45). The algebraic reconstruction technique algorithm was applied to each sinogram with 15 iteration cycles, and the 3D structure was obtained by stacking the reconstructed slices in order (46). Automatic 3D segmentation using the Avizo (Version 8.0.1, Visualization Science Group) was performed to calculate the sample volume at various pressures, which is proportional to the number of voxels within 3D segmentation.

**ACKNOWLEDGMENTS.** We thank Guoyin Shen for helpful discussions, and Bo Huang, Rongjie Xue, and Weixin Jiang for their help in the sample preparation. We thank Douglas Van Campen for his engineering support at BL6-2 Stanford Synchrotron Radiation Lightsources (SSRL). Initial TXM experiments were performed at beamline 13W, Shanghai Synchrotron Radiation Facility with the beamline support of Guangzhao Zhou. Portions of this research were carried out at the SSRL, a Directorate of SLAC National Accelerator Laboratory and an Office of Science User Facility operated for the US Department of Energy (DOE) Office of Science by Stanford University. The TXM sample preparation by FIB was performed at the Stanford Nano Shared Facilities (SNSF). We thank Sergey N. Tkachev for helping with the gas loading at sector 13, which is supported by the National Science Foundation (NSF) (EAR 11-57758 and EAR-1128799), the DOE (DE-FG02-94ER14466), and the Consortium for Materials Properties Research in Earth Sciences. Q.Z., W.Y., and H.-k.M. acknowledge financial support from the DOE-Basic Energy Sciences (BES) X-ray Scattering Core Program (DE-FG02-99ER45775) and from the National Natural Science Foundation of China (NSFC) (U1530402). W.L.M. and C.Y.S. are supported by NSF-EAR-1055454. W.H.W. is supported by NSFC (51271195). Use of the High Pressure Collaborative Access Team (HPCAT) facility is supported by the DOE-National Nuclear Security Administration under Award DE-NA0001974 and the DOE-BES under Award DE-FG02-99ER45775, with partial instrumentation funding by the NSF. The Advanced Photon Source is supported by the DOE-BES, under Contract DE-AC02-06CH11357.

- Greer AL (1995) Metallic glasses. *Science* 267(5206):1947–1953.
- Schroers J (2013) Bulk metallic glasses. *Phys Today* 66(2):32–37.
- Laws KJ, Miracle DB, Ferry M (2015) A predictive structural model for bulk metallic glasses. *Nat Commun* 6:8123.
- Greer AL (2015) New horizons for glass formation and stability. *Nat Mater* 14(6):542–546.
- Na JH, et al. (2014) Compositional landscape for glass formation in metal alloys. *Proc Natl Acad Sci USA* 111(25):9031–9036.
- Johnson WL, Samwer K (2005) A universal criterion for plastic yielding of metallic glasses with a  $(T/T_g)^{2/3}$  temperature dependence. *Phys Rev Lett* 95(19):195501.
- Liu YH, et al. (2009) Thermodynamic origins of shear band formation and the universal scaling law of metallic glass strength. *Phys Rev Lett* 103(6):065504.

- Wang WH (2006) Correlations between elastic moduli and properties in bulk metallic glasses. *J Appl Phys* 99(9):093506.
- Yang B, Liu CT, Nieh TG (2006) Unified equation for the strength of bulk metallic glasses. *Appl Phys Lett* 88(22):221911.
- Egami T, Poon SJ, Zhang Z, Keppens V (2007) Glass transition in metallic glasses: A microscopic model of topological fluctuations in the bonding network. *Phys Rev B* 76(2):024203.
- Martinez LM, Angell CA (2001) A thermodynamic connection to the fragility of glass-forming liquids. *Nature* 410(6829):663–667.
- Angell CA (1995) Formation of glasses from liquids and biopolymers. *Science* 267(5206):1924–1935.

13. Lewandowski JJ, Wang WH, Greer AL (2005) Intrinsic plasticity or brittleness of metallic glasses. *Philos Mag Lett* 85(2):77–87.
14. Schroers J, Johnson WL (2004) Ductile bulk metallic glass. *Phys Rev Lett* 93(25):255506.
15. Liu YH, et al. (2007) Super plastic bulk metallic glasses at room temperature. *Science* 315(5817):1385–1388.
16. Greaves GN, Greer AL, Lakes RS, Rouxel T (2011) Poisson's ratio and modern materials. *Nat Mater* 10(11):823–837.
17. Zeng Q, et al. (2011) Long-range topological order in metallic glass. *Science* 332(6036):1404–1406.
18. Sheng HW, Luo WK, Alamgir FM, Bai JM, Ma E (2006) Atomic packing and short-to-medium-range order in metallic glasses. *Nature* 439(7075):419–425.
19. Ma D, Stoica AD, Wang XL (2009) Power-law scaling and fractal nature of medium-range order in metallic glasses. *Nat Mater* 8(1):30–34.
20. Miracle DB (2004) A structural model for metallic glasses. *Nat Mater* 3(10):697–702.
21. Miracle DB, Egami T, Flores KM, Kelton KF (2007) Structural aspects of metallic glasses. *MRS Bull* 32(8):629–634.
22. Chen DZ, et al. (2015) Fractal atomic-level percolation in metallic glasses. *Science* 349(6254):1306–1310.
23. Cheng YQ, Ma E (2011) Atomic-level structure and structure-property relationship in metallic glasses. *Prog Mater Sci* 56(4):379–473.
24. Zeng Q, et al. (2014) Universal fractional noncubic power law for density of metallic glasses. *Phys Rev Lett* 112(18):185502.
25. Li Y, Guo Q, Kalb JA, Thompson CV (2008) Matching glass-forming ability with the density of the amorphous phase. *Science* 322(5909):1816–1819.
26. Wang WH (2007) Roles of minor additions in formation and properties of bulk metallic glasses. *Prog Mater Sci* 52(4):540–596.
27. Zeng QS, et al. (2010) Origin of pressure-induced polyamorphism in Ce75Al25 metallic glass. *Phys Rev Lett* 104(10):105702.
28. Sheng HW, et al. (2007) Polyamorphism in a metallic glass. *Nat Mater* 6(3):192–197.
29. Zeng QS, et al. (2009) Substitutional alloy of Ce and Al. *Proc Natl Acad Sci USA* 106(8):2515–2518.
30. Inoue A (2000) Stabilization of metallic supercooled liquid and bulk amorphous alloys. *Acta Mater* 48(1):279–306.
31. Hirata A, et al. (2011) Direct observation of local atomic order in a metallic glass. *Nat Mater* 10(1):28–33.
32. Poulsen HF, Wert JA, Neufeld J, Honkima V, Daymond M (2005) Measuring strain distributions in amorphous materials. *Nat Mater* 4(1):33–36.
33. Yavari AR, et al. (2005) Excess free volume in metallic glasses measured by X-ray diffraction. *Acta Mater* 53(6):1611–1619.
34. Zeng QS, et al. (2007) Anomalous compression behavior in lanthanum/cerium-based metallic glass under high pressure. *Proc Natl Acad Sci USA* 104(34):13565–13568.
35. Li G, Wang YY, Liaw PK, Li YC, Liu RP (2012) Electronic structure inheritance and pressure-induced polyamorphism in lanthanide-based metallic glasses. *Phys Rev Lett* 109(12):125501.
36. Sheng HW, Ma E, Liu HZ, Wen J (2006) Pressure tunes atomic packing in metallic glass. *Appl Phys Lett* 88(17):171906.
37. Cheng YQ, Sheng HW, Ma E (2008) Relationship between structure, dynamics, and mechanical properties in metallic glass-forming alloys. *Phys Rev B* 78(1):014207.
38. Miracle DB (2013) The density and packing fraction of binary metallic glasses. *Acta Mater* 61(9):3157–3171.
39. Scholze H (1991) *Glass: Nature, Structure, and Properties* (Springer, New York), 1st Ed, p 196.
40. Greer AL, Ma E (2007) Bulk metallic glasses: At the cutting edge of metals research. *MRS Bull* 32(8):611–615.
41. Egami T, Waseda Y (1984) Atomic size effect on the formability of metallic glasses. *J Non-Cryst Solids* 64(1–2):113–134.
42. Feder J, Jossang T, Rosenqvist E (1984) Scaling behavior and cluster fractal dimension determined by light-scattering from aggregating proteins. *Phys Rev Lett* 53(15):1403–1406.
43. Shante VKS, Kirkpatrick S (1971) An introduction to percolation theory. *Adv Phys* 20(85):325–357.
44. Mao HK, Bell PM, Shaner JW, Steinberg DJ (1978) Specific volume measurements of Cu, Mo, Pd, and Ag and calibration of ruby R1 fluorescence pressure gauge from 0.06 to 1 Mbar. *J Appl Phys* 49(6):3276–3283.
45. Liu Y, et al. (2012) TXM-Wizard: A program for advanced data collection and evaluation in full-field transmission X-ray microscopy. *J Synchrotron Radiat* 19(Pt 2):281–287.
46. Wang JY, et al. (2012) High pressure nano-tomography using an iterative method. *J Appl Phys* 111(11):112626.